SUPPORTING INFORMATION

Coordination Modulated Nonplanar Penta-Graphene as the Electronic Structural Lever for CO2RR Activity and Selectivity in Dual-Atom Catalysts

Yueyue Shao,[a,b] Huaying Zhong[a] and Jia Zhou[a,b,]*

[a] State Key Lab of Urban-rural Water Resource and Environment, School of Science, Harbin Institute of Technology, Shenzhen 518055, China

[b] School of Chemistry and Chemical Engineering, Harbin Institute of Technology, Harbin 150001, China

*Corresponding author E-mail:
jiazhou@hit.edu.cn

Supplementary Computational Section

The free-energy changes of the thermodynamic reaction pathway were evaluated using four elementary steps. The overall two-electron CO_2 reduction reactions are written as follows:

$$CO_2 + 2H^+ + 2e^- \rightarrow CO_{(g)} + H_2O_{(l)} \quad (S1)$$

$$CO_2 + 2H^+ + 2e^- \rightarrow HCOOH_{(l)} \quad (S2)$$

The corresponding elementary reactions and their Gibbs free-energy changes (ΔG_1, ΔG_2, ΔG_3, ΔG_4) of CO_2RR to CO (Equations S3-S6) and HCOOH (Equations S7-S10) are listed as follows:

$$* + CO_{2(g)} \rightarrow *CO_2 \quad (S3)$$

$$*CO_2 + H^+ + e^- \rightarrow *COOH \quad (S4)$$

$$*COOH + H^+ + e^- \rightarrow *CO + H_2O_{(l)} \quad (S5)$$

$$*CO \rightarrow * + CO_{(g)} \quad (S6)$$

$$* + CO_{2(g)} \rightarrow *CO_2 \quad (S7)$$

$$*CO_2 + H^+ + e^- \rightarrow *OCHO \quad (S8)$$

$$*OCHO + H^+ + e^- \rightarrow *HCOOH \quad (S9)$$

$$*HCOOH \rightarrow * + HCOOH_{(l)} \quad (S10)$$

where * refers to the active site on the surface of catalysts, the subscripts *g* and *l* stand for gas and liquid phases, respectively.

Formation energy E_f was defined as follows[1]:

$$E_f = (E_{PG-2TM} - E_{PG} - 2E_{TM})/2 \quad (S11)$$

In the above equation, E_{PG-2TM} and E_{PG} represent the total energy of the TM embedded structure and that of the PG substrate without embedded metal, respectively, while E_{TM} denotes the total energy per atom of the corresponding metal in its bulk phase.

The DOS projected onto the *d*-state that interacts with the adsorbate state can be characterized by the moments of the *d*-state DOS. The *d*-band center (ε_d) is calculated by[2]:

$$\varepsilon_d = \frac{\int_{-\infty}^{\infty} n_d(\varepsilon)\varepsilon d\varepsilon}{\int_{-\infty}^{\infty} n_d(\varepsilon) d\varepsilon} \quad \text{(S12)}$$

where ε and $n_d(\varepsilon)$ are the energy of *d*-state DOS and electronic density of *d*-state DOS, respectively.

The zero-point energy (ZPE) was calculated according to:

$$E_{ZPE} = \sum_{i=1}^{3N} \frac{hv_i}{2} \quad \text{(S13)}$$

The entropy change for adsorbed intermediates was calculated within the harmonic approximation:

$$\Delta S_{ads}(0 \rightarrow T, P^0) = S_{vib} = \sum_{i=1}^{3N} \left[\frac{N_A h v_i}{T(e^{hv_i/k_B T} - 1)} - Rln(1 - e^{-hv_i/k_B T}) \right] \quad \text{(S14)}$$

Where v_i is DFT-calculated normal-mode frequency for species of $3N$ degree of freedom (N = number of atoms) adsorbed on PG-based DACs, N_A is the Avogadro's constant, h is the Planck's constant, R is the ideal gas constant.

Supplementary Tables

Table S1. Summary of structural parameters (lattice length *a*, *b* and distance between two metal atoms) for 36 PG-based DACs, and the bond lengths of metal atoms in their bulk phase ($D_{m\text{-}m}$).[3]

PG-based DACs	*a* (Å)	*b* (Å)	$d_{m\text{-}m}$ (Å)	$D_{m\text{-}m}$ (Å)
$Sc_2NM\text{-}sp^2sp^3$	14.51	14.52	2.96	3.22
$Ti_2NM\text{-}sp^2sp^3$	14.51	14.51	2.88	2.98
$V_2FM\text{-}sp^2sp^3$	14.48	14.48	2.60	2.58
$Mn_2AFM\text{-}sp^2sp^3$	14.50	14.51	2.55	2.47
$Mn_2FM\text{-}sp^2sp^3$	14.49	14.50	2.72	2.47
$Fe_2AFM\text{-}sp^2sp^3$	14.52	14.51	2.10	2.43
$Fe_2FM\text{-}sp^2sp^3$	14.52	14.51	2.03	2.43
$Sc_2NM\text{-}sp^2sp^3sp^2\text{-}c$	14.43	14.51	2.93	3.22
$Ti_2NM\text{-}sp^2sp^3sp^2\text{-}c$	14.43	14.50	2.60	2.98
$V_2NM\text{-}sp^2sp^3sp^2\text{-}c$	14.47	14.50	2.20	2.58
$Cr_2AFM\text{-}sp^2sp^3sp^2\text{-}c$	14.44	14.48	2.24	2.46
$Cr_2FM\text{-}sp^2sp^3sp^2\text{-}c$	14.43	14.50	2.40	2.46
$Mn_2AFM\text{-}sp^2sp^3sp^2\text{-}c$	14.46	14.48	2.37	2.47
$Mn_2FM\text{-}sp^2sp^3sp^2\text{-}c$	14.44	14.48	2.44	2.47
$Fe_2AFM\text{-}sp^2sp^3sp^2\text{-}c$	14.44	14.80	2.25	2.43
$Fe_2FM\text{-}sp^2sp^3sp^2\text{-}c$	14.46	14.48	2.27	2.43
$Co_2AFM\text{-}sp^2sp^3sp^2\text{-}c$	14.46	14.48	2.24	2.48
$Co_2FM\text{-}sp^2sp^3sp^2\text{-}c$	14.43	14.48	2.20	2.48
$Ni_2NM\text{-}sp^2sp^3sp^2\text{-}c$	14.47	14.46	2.38	2.49
$Cu_2NM\text{-}sp^2sp^3sp^2\text{-}c$	14.48	14.45	2.52	2.57
$Ti_2NM\text{-}sp^2sp^3sp^2\text{-}t$	14.54	14.54	2.60	2.98
$V_2AFM\text{-}sp^2sp^3sp^2\text{-}t$	14.53	14.42	2.34	2.58
$V_2FM\text{-}sp^2sp^3sp^2\text{-}t$	14.52	14.42	2.37	2.58
$Mn_2AFM\text{-}sp^2sp^3sp^2\text{-}t$	14.50	14.47	2.31	2.47
$Mn_2FM\text{-}sp^2sp^3sp^2\text{-}t$	14.52	14.46	2.38	2.47
$Co_2NM\text{-}sp^2sp^3sp^2\text{-}t$	14.50	14.46	2.30	2.43
$Ti_2FM\text{-}sp^3sp^2sp^3$	14.53	14.47	2.66	2.43
$V_2NM\text{-}sp^3sp^2sp^3$	14.54	14.56	2.48	2.58
$Cr_2AFM\text{-}sp^3sp^2sp^3$	14.53	14.53	2.58	2.46
$Cr_2FM\text{-}sp^3sp^2sp^3$	14.48	14.54	2.59	2.46
$Mn_2AFM\text{-}sp^3sp^2sp^3$	14.49	14.53	2.31	2.47
$Mn_2FM\text{-}sp^3sp^2sp^3$	14.48	14.51	2.49	2.47
$Fe_2AFM\text{-}sp^3sp^2sp^3$	14.50	14.51	2.23	2.43
$Fe_2FM\text{-}sp^3sp^2sp^3$	14.51	14.51	2.22	2.43
$Co_2NM\text{-}sp^3sp^2sp^3$	14.53	14.53	2.30	2.43
$Ni_2NM\text{-}sp^3sp^2sp^3$	14.53	14.53	2.22	2.49

Table S2. Free energy corrections including zero-point energy (ZPE) and entropy (S) for gas-phase species.

Molecular	ZPE (eV)	T × S (eV)
CO_2	0.31	0.66
CO	0.14	0.67
H_2	0.31	0.40
H_2O	0.57	0.66
HCOOH	0.90	1.02

Table S3. Overpotential for 35 catalytically evaluable PG-based DACs to produce CO, HCOOH and H_2 with two-electron transfer reactions in aqueous electrolytes.

PG-based DACs	η^{CO} (V)	η^{HCOOH} (V)	η^{H2} (V)
Sc_2NM-sp^2sp^3	0.621	0.504	1.329
Ti_2NM-sp^2sp^3	0.857	0.659	0.209
V_2FM-sp^2sp^3	0.960	0.591	0.215
Mn_2AFM-sp^2sp^3	0.782	0.193	0.382
Mn_2FM-sp^2sp^3	0.933	0.157	0.366
Fe_2AFM-sp^2sp^3	0.914	1.108	1.556
Fe_2FM-sp^2sp^3	0.752	0.752	1.396
Sc_2NM-$sp^2sp^3sp^2$-c	0.375	0.676	0.585
Ti_2NM-$sp^2sp^3sp^2$-c	0.845	0.660	0.194
V_2NM-$sp^2sp^3sp^2$-c	0.917	0.749	0.239
Cr_2AFM-$sp^2sp^3sp^2$-c	0.896	0.420	0.291
Cr_2FM-$sp^2sp^3sp^2$-c	0.978	0.464	0.184
Mn_2AFM-$sp^2sp^3sp^2$-c	0.569	0.265	0.275
Mn_2FM-$sp^2sp^3sp^2$-c	1.147	0.276	0.292
Fe_2AFM-$sp^2sp^3sp^2$-c	1.320	0.138	0.165
Fe_2FM-$sp^2sp^3sp^2$-c	1.097	0.091	0.286
Co_2AFM-$sp^2sp^3sp^2$-c	1.347	0.233	0.043
Co_2FM-$sp^2sp^3sp^2$-c	1.418	0.167	0.018
Ni_2NM-$sp^2sp^3sp^2$-c	0.734	0.913	0.131
Cu_2NM-$sp^2sp^3sp^2$-c	0.527	1.047	0.615
V_2AFM-$sp^2sp^3sp^2$-t	1.491	0.776	0.094
V_2FM-$sp^2sp^3sp^2$-t	1.468	0.930	0.076
Mn_2AFM-$sp^2sp^3sp^2$-t	1.381	0.309	0.198
Mn_2FM-$sp^2sp^3sp^2$-t	1.609	0.357	0.073
Co_2NM-$sp^2sp^3sp^2$-t	1.480	0.463	0.228
Ti_2FM-$sp^3sp^2sp^3$	0.952	0.647	0.268
V_2NM-$sp^3sp^2sp^3$	0.439	0.362	0.702
Cr_2AFM-$sp^3sp^2sp^3$	0.588	0.314	0.835
Cr_2FM-$sp^3sp^2sp^3$	0.555	0.362	0.405
Mn_2AFM-$sp^3sp^2sp^3$	0.556	0.166	0.570
Mn_2FM-$sp^3sp^2sp^3$	0.605	0.179	0.593
Fe_2AFM-$sp^3sp^2sp^3$	0.631	0.151	0.598
Fe_2FM-$sp^3sp^2sp^3$	0.632	0.178	0.708
Co_2NM-$sp^3sp^2sp^3$	0.896	0.253	1.395
Ni_2NM-$sp^3sp^2sp^3$	1.137	0.577	0.404

Table S4. The 16 selected descriptors of 35 catalytically evaluable PG-based DACs retained for detailed CO_2RR analysis.

PG-based DACs	Q_{TM}	ε_d	ICOHP	Z
Sc_2NM-sp^2sp^3	1.700	1.489	-0.103	21
Ti_2NM-sp^2sp^3	1.571	1.129	-0.136	22
V_2FM-sp^2sp^3	1.418	0.220	-0.328	23
Mn_2AFM-sp^2sp^3	1.076	-0.674	-0.173	25
Mn_2FM-sp^2sp^3	1.098	-0.494	-0.077	25
Fe_2AFM-sp^2sp^3	0.801	-0.783	-1.465	26
Fe_2FM-sp^2sp^3	0.766	-0.644	-1.581	26
Sc_2NM-$sp^2sp^3sp^2$-c	1.639	1.692	-0.131	21
Ti_2NM-$sp^2sp^3sp^2$-c	1.520	0.888	-0.369	22
V_2NM-$sp^2sp^3sp^2$-c	1.257	0.412	-1.094	23
Cr_2AFM-$sp^2sp^3sp^2$-c	1.084	0.056	-0.749	24
Cr_2FM-$sp^2sp^3sp^2$-c	1.131	0.070	-0.422	24
Mn_2AFM-$sp^2sp^3sp^2$-c	0.922	-0.775	-0.361	25
Mn_2FM-$sp^2sp^3sp^2$-c	0.998	-0.572	-0.213	25
Fe_2AFM-$sp^2sp^3sp^2$-c	0.800	-1.601	-0.328	26
Fe_2FM-$sp^2sp^3sp^2$-c	0.831	-1.410	-0.331	26
Co_2AFM-$sp^2sp^3sp^2$-c	0.643	-1.575	-0.183	27
Co_2FM-$sp^2sp^3sp^2$-c	0.639	-1.382	-0.206	27
Ni_2NM-$sp^2sp^3sp^2$-c	0.581	-2.367	-0.044	28
Cu_2NM-$sp^2sp^3sp^2$-c	0.550	-2.400	0.004	29
V_2AFM-$sp^2sp^3sp^2$-t	1.192	0.332	-0.732	23
V_2FM-$sp^2sp^3sp^2$-t	1.205	0.362	-0.665	23
Mn_2AFM-$sp^2sp^3sp^2$-t	0.864	-0.745	-0.620	25
Mn_2FM-$sp^2sp^3sp^2$-t	0.868	-0.630	-0.344	25
Co_2NM-$sp^2sp^3sp^2$-t	0.595	-1.980	-0.192	27
Ti_2FM-$sp^3sp^2sp^3$	1.644	1.134	-0.220	22
V_2NM-$sp^3sp^2sp^3$	1.453	0.141	-0.432	23
Cr_2AFM-$sp^3sp^2sp^3$	1.269	-0.447	-0.185	24
Cr_2FM-$sp^3sp^2sp^3$	1.261	-0.514	-0.223	24
Mn_2AFM-$sp^3sp^2sp^3$	1.045	-0.824	-0.478	25
Mn_2FM-$sp^3sp^2sp^3$	1.069	-0.842	-0.127	25
Fe_2AFM-$sp^3sp^2sp^3$	0.771	-1.420	-0.283	26
Fe_2FM-$sp^3sp^2sp^3$	0.786	-1.388	-0.321	26
Co_2NM-$sp^3sp^2sp^3$	0.684	-2.638	-0.086	27
Ni_2NM-$sp^3sp^2sp^3$	0.562	-2.750	-0.084	28

PG-based DACs	P	IE_1	W_M	E_M
Sc_2NM-sp^2sp^3	1.36	6.56	3.50	3.90
Ti_2NM-sp^2sp^3	1.54	6.82	4.33	4.85
V_2FM-sp^2sp^3	1.63	6.74	4.30	5.31
Mn_2AFM-sp^2sp^3	1.55	7.43	4.10	2.92
Mn_2FM-sp^2sp^3	1.55	7.43	4.10	2.92
Fe_2AFM-sp^2sp^3	1.83	7.87	4.81	4.28
Fe_2FM-sp^2sp^3	1.83	7.87	4.81	4.28
Sc_2NM-$sp^2sp^3sp^2$-c	1.36	6.56	3.50	3.90
Ti_2NM-$sp^2sp^3sp^2$-c	1.54	6.82	4.33	4.85
V_2NM-$sp^2sp^3sp^2$-c	1.63	6.74	4.30	5.31
Cr_2AFM-$sp^2sp^3sp^2$-c	1.66	6.77	4.50	4.10
Cr_2FM-$sp^2sp^3sp^2$-c	1.66	6.77	4.50	4.10
Mn_2AFM-$sp^2sp^3sp^2$-c	1.55	7.43	4.10	2.92
Mn_2FM-$sp^2sp^3sp^2$-c	1.55	7.43	4.10	2.92
Fe_2AFM-$sp^2sp^3sp^2$-c	1.83	7.87	4.81	4.28
Fe_2FM-$sp^2sp^3sp^2$-c	1.83	7.87	4.81	4.28
Co_2AFM-$sp^2sp^3sp^2$-c	1.88	7.88	5.00	4.39
Co_2FM-$sp^2sp^3sp^2$-c	1.88	7.88	5.00	4.39
Ni_2NM-$sp^2sp^3sp^2$-c	1.91	7.63	5.35	4.44
Cu_2NM-$sp^2sp^3sp^2$-c	1.9	7.72	5.10	3.49
V_2AFM-$sp^2sp^3sp^2$-t	1.63	6.74	4.30	5.31
V_2FM-$sp^2sp^3sp^2$-t	1.63	6.74	4.30	5.31
Mn_2AFM-$sp^2sp^3sp^2$-t	1.55	7.43	4.10	2.92
Mn_2FM-$sp^2sp^3sp^2$-t	1.55	7.43	4.10	2.92
Co_2NM-$sp^2sp^3sp^2$-t	1.88	7.88	5.00	4.39
Ti_2FM-$sp^3sp^2sp^3$	1.54	6.82	4.33	4.85
V_2NM-$sp^3sp^2sp^3$	1.63	6.74	4.30	5.31
Cr_2AFM-$sp^3sp^2sp^3$	1.66	6.77	4.50	4.10
Cr_2FM-$sp^3sp^2sp^3$	1.66	6.77	4.50	4.10
Mn_2AFM-$sp^3sp^2sp^3$	1.55	7.43	4.10	2.92
Mn_2FM-$sp^3sp^2sp^3$	1.55	7.43	4.10	2.92
Fe_2AFM-$sp^3sp^2sp^3$	1.83	7.87	4.81	4.28
Fe_2FM-$sp^3sp^2sp^3$	1.83	7.87	4.81	4.28
Co_2NM-$sp^3sp^2sp^3$	1.88	7.88	5.00	4.39
Ni_2NM-$sp^3sp^2sp^3$	1.91	7.63	5.35	4.44

PG-based DACs	r_{atomic}	V_{atomic}	m	N_s
$Sc_2NM\text{-}sp^2sp^3$	1.44	12.57	44.96	2
$Ti_2NM\text{-}sp^2sp^3$	1.47	10.63	47.87	2
$V_2FM\text{-}sp^2sp^3$	1.53	9.83	50.94	2
$Mn_2AFM\text{-}sp^2sp^3$	1.39	8.06	54.94	2
$Mn_2FM\text{-}sp^2sp^3$	1.39	8.06	54.94	2
$Fe_2AFM\text{-}sp^2sp^3$	1.32	7.11	55.85	2
$Fe_2FM\text{-}sp^2sp^3$	1.32	7.11	55.85	2
$Sc_2NM\text{-}sp^2sp^3sp^2\text{-}c$	1.44	12.57	44.96	2
$Ti_2NM\text{-}sp^2sp^3sp^2\text{-}c$	1.47	10.63	47.87	2
$V_2NM\text{-}sp^2sp^3sp^2\text{-}c$	1.53	9.83	50.94	2
$Cr_2AFM\text{-}sp^2sp^3sp^2\text{-}c$	1.52	8.65	52	2
$Cr_2FM\text{-}sp^2sp^3sp^2\text{-}c$	1.52	8.65	52	2
$Mn_2AFM\text{-}sp^2sp^3sp^2\text{-}c$	1.39	8.06	54.94	2
$Mn_2FM\text{-}sp^2sp^3sp^2\text{-}c$	1.39	8.06	54.94	2
$Fe_2AFM\text{-}sp^2sp^3sp^2\text{-}c$	1.32	7.11	55.85	2
$Fe_2FM\text{-}sp^2sp^3sp^2\text{-}c$	1.32	7.11	55.85	2
$Co_2AFM\text{-}sp^2sp^3sp^2\text{-}c$	1.26	6.61	58.93	2
$Co_2FM\text{-}sp^2sp^3sp^2\text{-}c$	1.26	6.61	58.93	2
$Ni_2NM\text{-}sp^2sp^3sp^2\text{-}c$	1.24	6.59	58.69	2
$Cu_2NM\text{-}sp^2sp^3sp^2\text{-}c$	1.28	6.53	63.55	2
$V_2AFM\text{-}sp^2sp^3sp^2\text{-}t$	1.53	9.83	50.94	2
$V_2FM\text{-}sp^2sp^3sp^2\text{-}t$	1.53	9.83	50.94	2
$Mn_2AFM\text{-}sp^2sp^3sp^2\text{-}t$	1.39	8.06	54.94	2
$Mn_2FM\text{-}sp^2sp^3sp^2\text{-}t$	1.39	8.06	54.94	2
$Co_2NM\text{-}sp^2sp^3sp^2\text{-}t$	1.26	6.61	58.93	2
$Ti_2FM\text{-}sp^3sp^2sp^3$	1.47	10.63	47.87	2
$V_2NM\text{-}sp^3sp^2sp^3$	1.53	9.83	50.94	2
$Cr_2AFM\text{-}sp^3sp^2sp^3$	1.52	8.65	52.00	2
$Cr_2FM\text{-}sp^3sp^2sp^3$	1.52	8.65	52.00	2
$Mn_2AFM\text{-}sp^3sp^2sp^3$	1.39	8.06	54.94	2
$Mn_2FM\text{-}sp^3sp^2sp^3$	1.39	8.06	54.94	2
$Fe_2AFM\text{-}sp^3sp^2sp^3$	1.32	7.11	55.85	2
$Fe_2FM\text{-}sp^3sp^2sp^3$	1.32	7.11	55.85	2
$Co_2NM\text{-}sp^3sp^2sp^3$	1.26	6.61	58.93	2
$Ni_2NM\text{-}sp^3sp^2sp^3$	1.24	6.59	58.69	2

PG-based DACs	N_d	$N_{valence}$	$Bond_{TM1-TM2}$	ΔG_{*CO2}
Sc_2NM-sp^2sp^3	1	3	2.964	-0.485
Ti_2NM-sp^2sp^3	2	4	2.879	-0.557
V_2FM-sp^2sp^3	3	5	2.597	-0.212
Mn_2AFM-sp^2sp^3	5	7	2.554	-0.234
Mn_2FM-sp^2sp^3	5	7	2.724	-0.177
Fe_2AFM-sp^2sp^3	6	8	2.100	0.9136
Fe_2FM-sp^2sp^3	6	8	2.031	0.752
Sc_2NM-$sp^2sp^3sp^2$-c	1	3	2.927	-0.423
Ti_2NM-$sp^2sp^3sp^2$-c	2	4	2.603	-0.518
V_2NM-$sp^2sp^3sp^2$-c	3	5	2.198	-0.537
Cr_2AFM-$sp^2sp^3sp^2$-c	4	6	2.238	-0.390
Cr_2FM-$sp^2sp^3sp^2$-c	4	6	2.401	-0.474
Mn_2AFM-$sp^2sp^3sp^2$-c	5	7	2.368	-0.237
Mn_2FM-$sp^2sp^3sp^2$-c	5	7	2.443	-0.362
Fe_2AFM-$sp^2sp^3sp^2$-c	6	8	2.250	-0.324
Fe_2FM-$sp^2sp^3sp^2$-c	6	8	2.265	-0.171
Co_2AFM-$sp^2sp^3sp^2$-c	7	9	2.239	-0.567
Co_2FM-$sp^2sp^3sp^2$-c	7	9	2.198	-0.430
Ni_2NM-$sp^2sp^3sp^2$-c	8	10	2.377	-0.215
Cu_2NM-$sp^2sp^3sp^2$-c	9	11	2.522	-0.052
V_2AFM-$sp^2sp^3sp^2$-t	3	5	2.336	-0.622
V_2FM-$sp^2sp^3sp^2$-t	3	5	2.365	-0.623
Mn_2AFM-$sp^2sp^3sp^2$-t	5	7	2.311	-0.337
Mn_2FM-$sp^2sp^3sp^2$-t	5	7	2.379	-0.373
Co_2NM-$sp^2sp^3sp^2$-t	7	9	2.302	-0.601
Ti_2FM-$sp^3sp^2sp^3$	2	4	2.659	-0.32
V_2NM-$sp^3sp^2sp^3$	3	5	2.478	-0.116
Cr_2AFM-$sp^3sp^2sp^3$	4	6	2.583	-0.133
Cr_2FM-$sp^3sp^2sp^3$	4	6	2.587	-0.239
Mn_2AFM-$sp^3sp^2sp^3$	5	7	2.306	-0.198
Mn_2FM-$sp^3sp^2sp^3$	5	7	2.489	-0.065
Fe_2AFM-$sp^3sp^2sp^3$	6	8	2.232	-0.091
Fe_2FM-$sp^3sp^2sp^3$	6	8	2.216	-0.121
Co_2NM-$sp^3sp^2sp^3$	7	9	2.304	-0.306
Ni_2NM-$sp^3sp^2sp^3$	8	10	2.217	-0.170

Table S5. Structural and electronic descriptors used as input features in the machine learning models for PG-based DACs.

Symbol	Descriptor
Q_{TM}	Bader charge of dual-atom center
ε_d	*d*-band center of dual-atom center
ICOHP	Integrated crystal orbital Hamilton population of dual-atom center
Z	Atomic number
P	Electronegativity
IE_1	First ionization energy
W_M	Work function of metal
E_M	Cohesive energy of metal
r_{atomic}	Atomic radius
V_{atomic}	Molar atomic volume
m	Relative atomic mass
N_s	Valence *s* electron count
N_d	Valence *d*-electron count
$N_{valence}$	Total valence electron count
$Bond_{TM1\text{-}TM2}$	Metal-metal distance at active site
ΔG_{*CO2}	CO_2 adsorption free energy

Note: Elemental quantities (Z, P, IE_1, W_M, E_M, r_{atomic}, V_{atomic}, m, N_s, N_d, $N_{valence}$) are taken from standard elemental data for the corresponding transition metal, while site specific quantities (Q_{TM}, ε_d, ICOHP, $Bond_{TM1\text{-}TM2}$, ΔG_{*CO2}) are obtained from DFT

calculations of the PG-based DACs.

Table S6. Machine-learning models and hyperparameters.

Model	Implementation summary	Hyperparameters
Poly-Ridge	Polynomial feature expansion + standardization + Ridge regression	degree = 2 include_bias = False interaction_only = False alpha = 1.631 solver = saga max_iter = 20000 random_state = 42
RBF-NuSVR	Standardization + ν-support vector regression with RBF kernel	C = 5.829 nu = 0.759 gamma = 0.026
Note	A Yeo–Johnson transformation was applied to the target variable during fitting of the RBF-NuSVR model	

Supplementary Figures

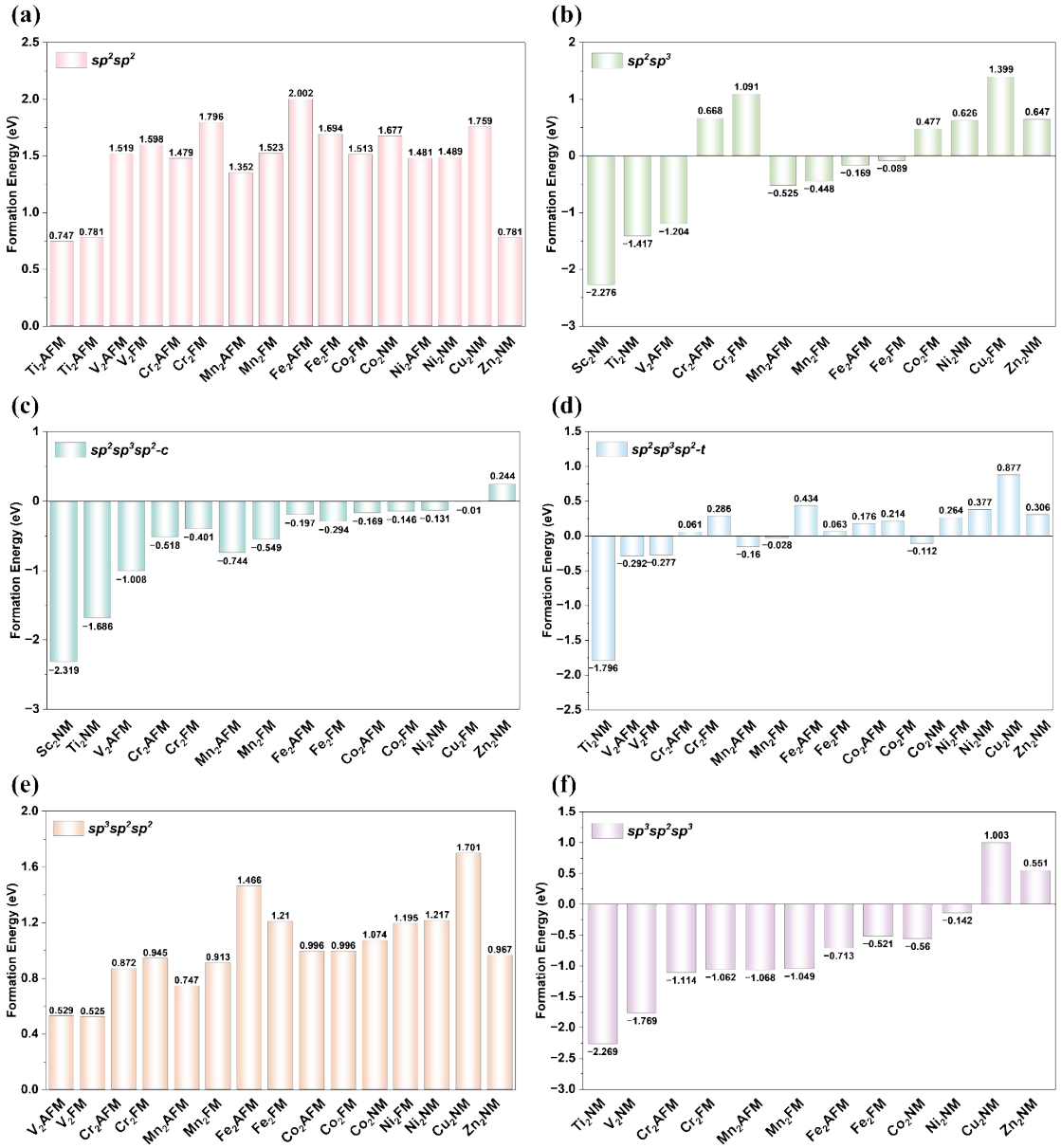

Figure S1. Formation energies of 86 PG-based DACs relative to the vacant PG substrate and bulk metal reference.

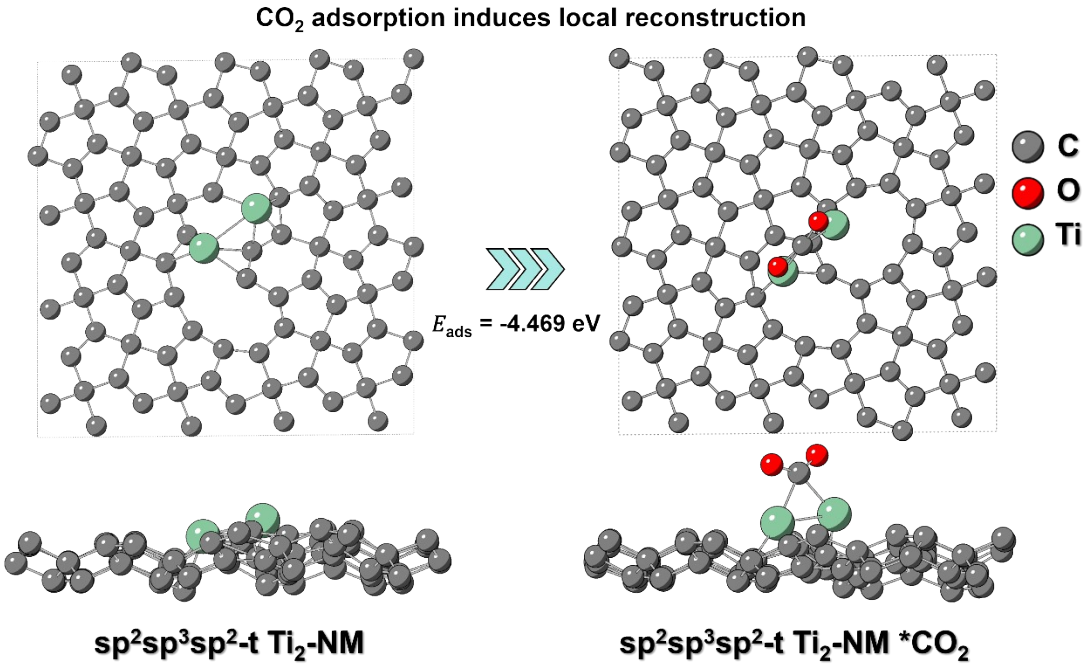

Figure S2. Structural evolution of $sp^2sp^3sp^2$-t Ti_2-NM upon CO_2 adsorption.

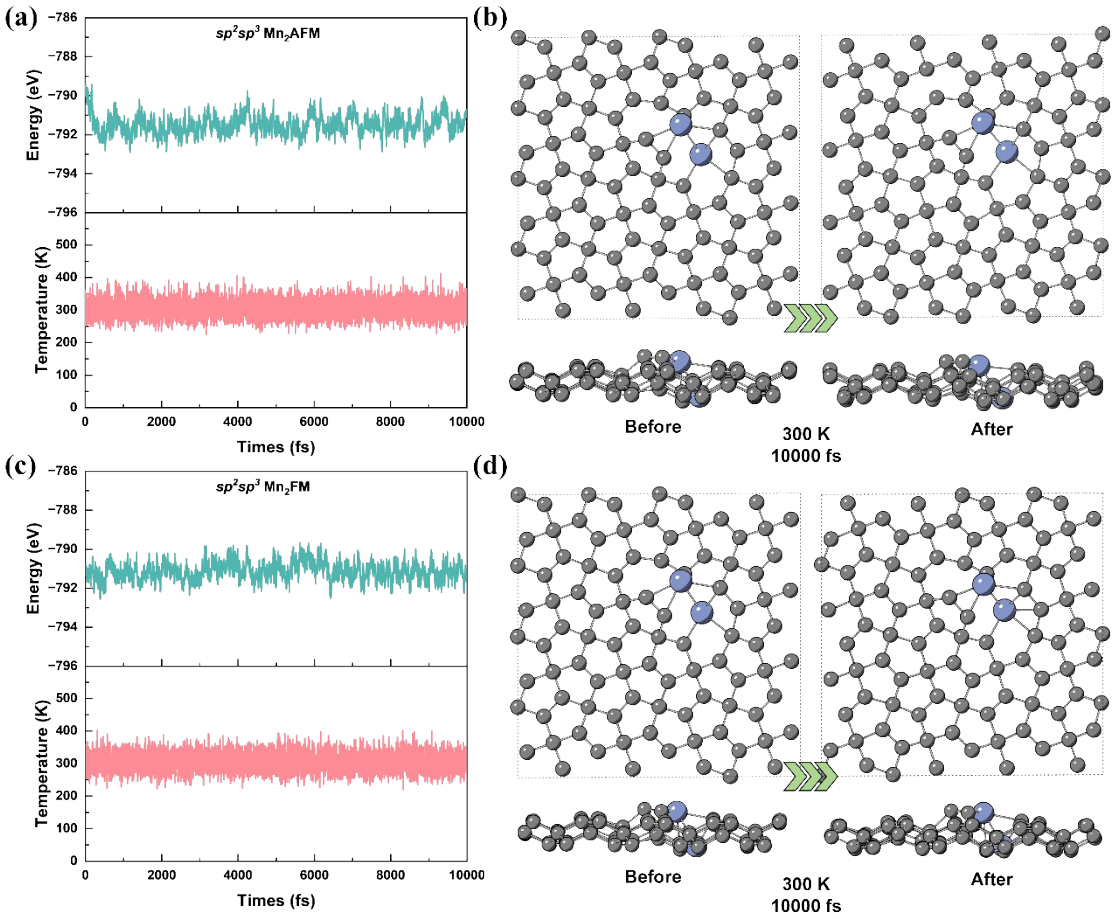

Figure S3. (a) and (c) Variation of total energy and temperature of PG-based sp^2sp^3 Mn_2AFM and Mn_2FM for 10000 fs during MD simulation at 300 K; (b) and (d) The Geometry snapshot of the initial and final states of PG-based sp^2sp^3 Mn_2AFM and Mn_2FM.

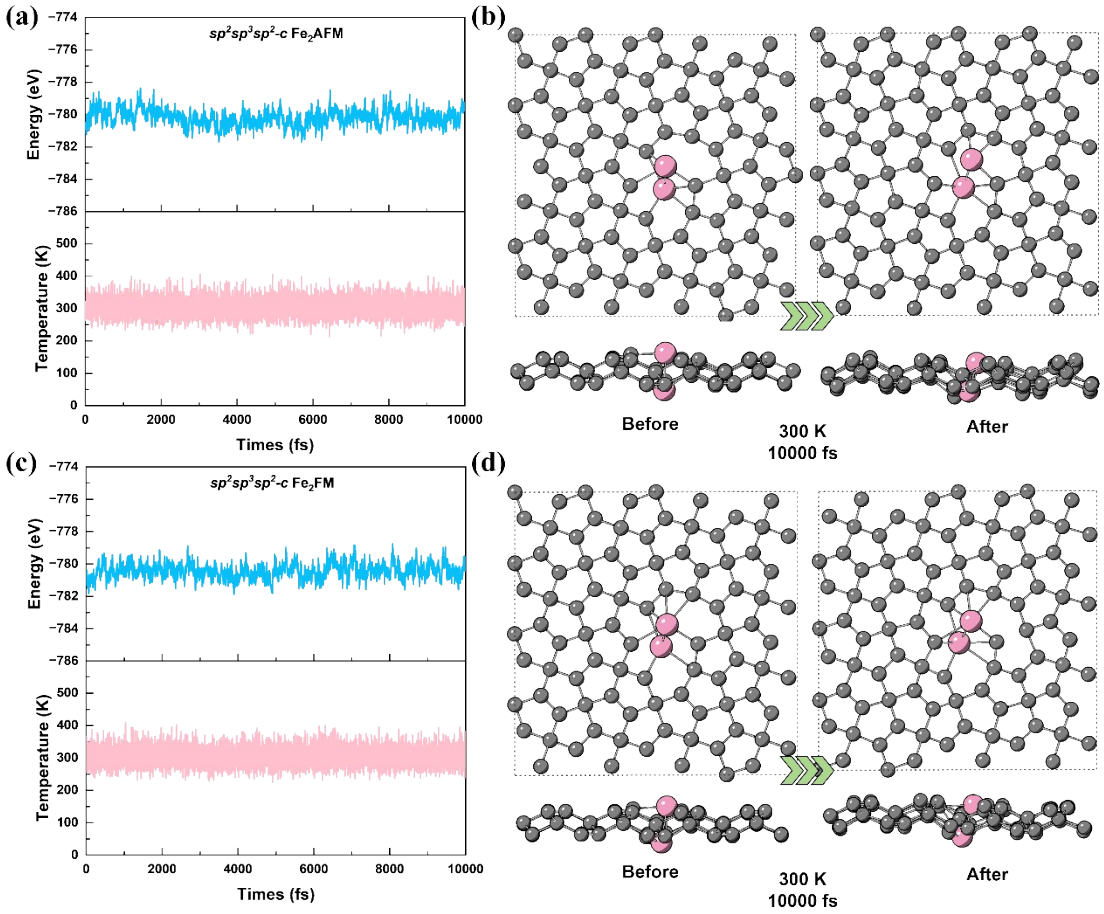

Figure S4. (a) and (c) Variation of total energy and temperature of PG-based $sp^2sp^3sp^2$-c Fe_2AFM and Fe_2FM for 10000 fs during MD simulation at 300 K; (b) and (d) The Geometry snapshot of the initial and final states of PG-based $sp^2sp^3sp^2$-c Fe_2AFM and Fe_2FM.

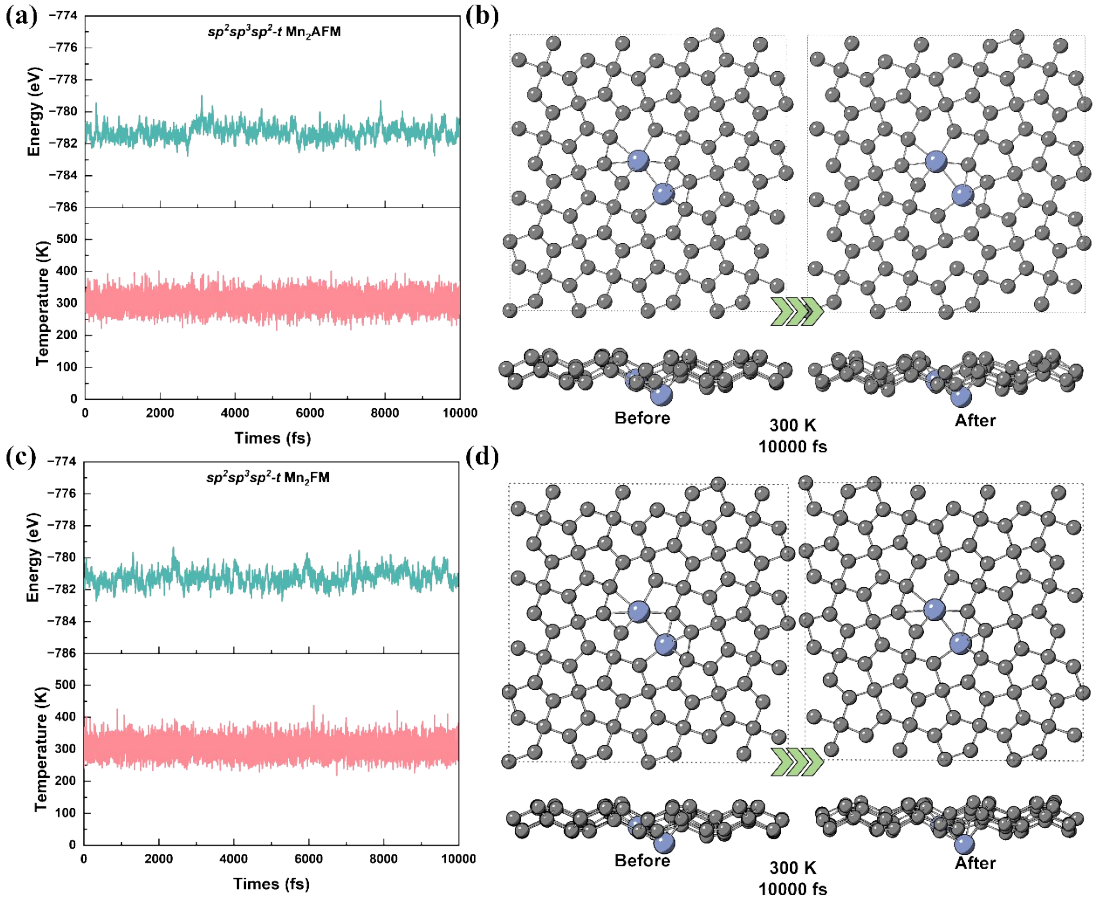

Figure S5. (a) and (c) Variation of total energy and temperature of PG-based $sp^2sp^3sp^2$-t Mn_2AFM and Mn_2FM for 10000 fs during MD simulation at 300 K; (b) and (d) The Geometry snapshot of the initial and final states of PG-based $sp^2sp^3sp^2$-t Mn_2AFM and Mn_2FM.

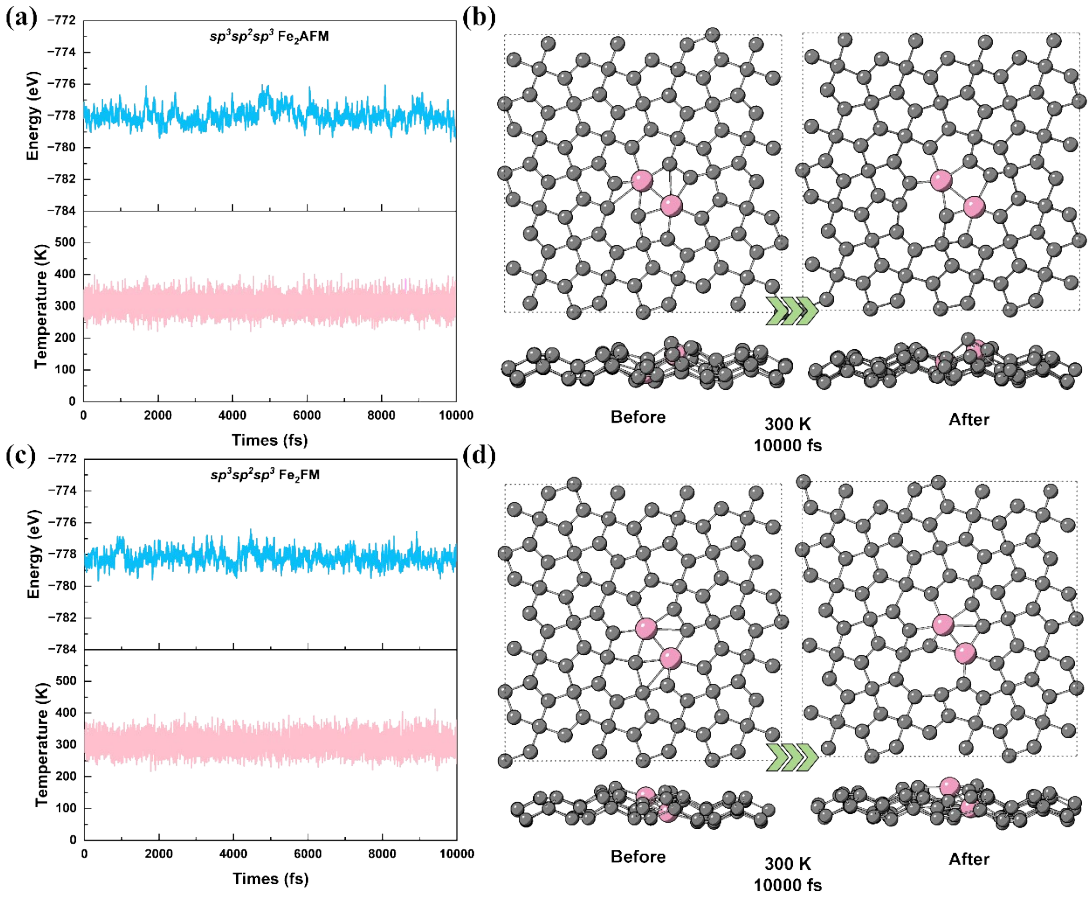

Figure S6. (a) and (c) Variation of total energy and temperature of PG-based $sp^3sp^2sp^3$ Fe_2AFM and Fe_2FM for 10000 fs during MD simulation at 300 K; (b) and (d) The Geometry snapshot of the initial and final states of PG-based $sp^3sp^2sp^3$ Fe_2AFM and Fe_2FM.

References

(1) Kattel, S.; Atanassov, P.; Kiefer, B. A density functional theory study of oxygen reduction reaction on non-PGM Fe-N-C electrocatalysts. *Phys. Chem. Chem. Phys.* **2014**, *16* (27), 13800–13806.

(2) Norskov, J. K.; Abild-Pedersen, F.; Studt, F.; Bligaard, T. Density functional theory in surface chemistry and catalysis. *Proc. Natl. Acad. Sci. U. S. A.* **2011**, *108* (3), 937–943.

(3) Guo, X.; Gu, J.; Lin, S.; Zhang, S.; Chen, Z.; Huang, S. Tackling the activity and selectivity challenges of electrocatalysts toward the nitrogen reduction reaction via atomically dispersed biatom catalysts. *J. Am. Chem. Soc.* **2020**, *142* (12), 5709–5721.